Recycling Ambient Microwave Energy With Broad-Band Rectenna Arrays

Joseph A. Hagerty, *Student Member, IEEE*, Florian B. Helmbrecht, *Student Member, IEEE*, William H. McCalpin, *Student Member, IEEE*, Regan Zane, *Member, IEEE*, and Zoya B. Popović, *Fellow, IEEE*

Abstract—This paper presents a study of reception and rectification of broad-band statistically time-varying low-power-density microwave radiation. The applications are in wireless powering of industrial sensors and recycling of ambient RF energy. A 64-element dual-circularly-polarized spiral rectenna array is designed and characterized over a frequency range of 2–18 GHz with single-tone and multitone incident waves. The integrated design of the antenna and rectifier, using a combination of full-wave electromagnetic field analysis and harmonic balance nonlinear circuit analysis, eliminates matching and filtering circuits, allowing for a compact element design. The rectified dc power and efficiency is characterized as a function of dc load and dc circuit topology, RF frequency, polarization, and incidence angle for power densities between 10^{-5}–10^{-1} mW/cm^2. In addition, the increase in rectenna efficiency for multitone input waves is presented.

Index Terms—DC–DC conversion, power combining, rectenna, rectifier.

I. INTRODUCTION

RECTIFICATION of microwave signals for supplying dc power through wireless transmission has been proposed and researched in the context of high-power beaming since the 1950s, a good review of which is given in [1]. In microwave power transmission, the antennas have well-defined polarization and high rectification efficiency enabled by single-frequency, high microwave power densities incident on an array of antennas and rectifying circuits. Applications for this type of power transfer have been proposed for helicopter powering [1], solar-powered satellite-to-ground transmission [2], intersatellite power transmission [3], [4] including utility power satellites [5], mechanical actuators for space-based telescopes [6], small dc motor driving [7], and short-range wireless power transfer, e.g., between two parts of a satellite. Linear [8], [9] dual-linear [6], [10], and circular polarization [2], [11] of the receiving antennas were used for demonstrations of efficiencies ranging from around 85%–90% at lower

microwave frequencies to around 60% at the X-band and around 40% at the Ka-band [5]. Additional applications for short distances are in the area-active RF identification (RFID) tags, where narrow-band electrically small antennas are used, e.g., [12], [13], and in biomedical implants, e.g., [14], [15].

In the above referenced work, rectification was performed for narrow-band, essentially single-frequency, incident microwave radiation with relatively high power densities. A survey of the typical power densities associated with high-power rectennas is given in Fig. 1, in which three examples are taken from [3], [6], and [8] along with the corresponding operating rectification efficiencies. Also shown in the figure are expected power densities near a typical base-station tower operating at 880 and 1990 MHz [16]. Concerns have been expressed in terms of possible health hazards [17]. In [8], rectification of low power levels was discussed for battery-free transponders, with power densities on the order of 10^{-2} mW/cm^2. More recently, broad-band rectification of very low-power incident radiation (less than 1 mW/cm^2) was demonstrated in [18].

This paper focuses on incident power densities and input power levels that are orders of magnitude lower than those associated with the projects in the literature cited above. Simulation, design and performance of a broad-band rectenna array (tested from 2 to 18 GHz) for rectification of low-power (10^{-5}–10^{-1} mW/cm^2), arbitrarily polarized incident radiation is presented. The work is motivated by two types of applications: powering of low-power indoor sensor networks and RF energy recycling. Because of the low input power levels, a nonlinear decrease in efficiency is expected when compared to power-beaming applications. The goal of this work is to determine the usefulness of low-power rectification.

The general block diagram of the rectenna array discussed in this paper is shown in Fig. 2. Multiple sources of different frequencies are radiating power in all directions in a rich scattering environment. The dc powers from many rectenna elements are added by current and voltage summing with a conversion efficiency

$$\eta = \frac{P_{\text{dc}}}{P_{\text{RF}}} \tag{1}$$

which is a function of statistically varying incident RF power, $\eta = \eta(P_{\text{RF}})$. The received average RF power over a range of frequencies at any instant in time is given by

$$P_{\text{RF}}(t) = \frac{1}{f_2 - f_1} \int_{f_1}^{f_2} \int_0^{4\pi} S(\Omega, f, t) A_{\text{eff}}(\Omega, f) d\Omega df \tag{2}$$

where Ω is the solid angle in steradians and $S(\Omega, f, t)$ is the time-varying frequency and angle-dependent incident power
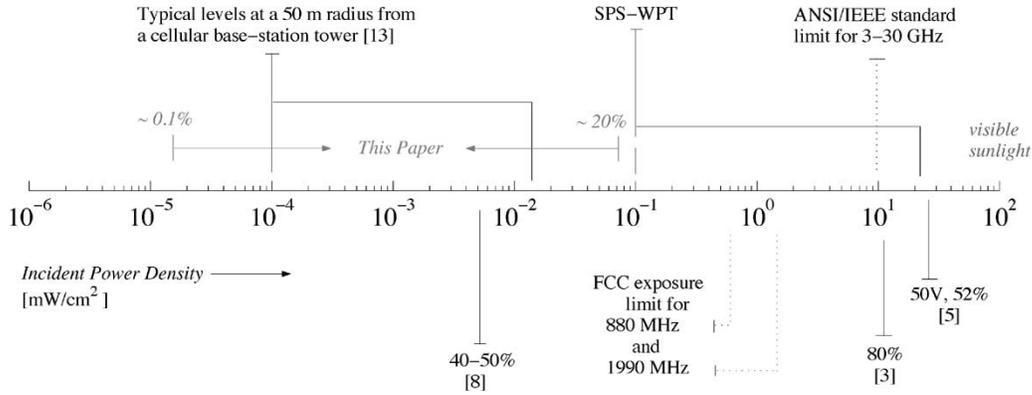
Fig. 1. Diagram of various microwave power sources and their typical power density levels. The power density operating points of several rectenna designs found in the literature and their corresponding efficiencies [3], [6], [8] are given. Also shown is the range of expected power densities used in the solar power satellite (SPS) and wireless power transmission (WPT) applications. The range of power densities measured in this paper is indicated for comparison. Measured ambient levels in our laboratory (no high-power equipment) are in the 10^{-6}–10^{-5}-mW/cm^2 range.
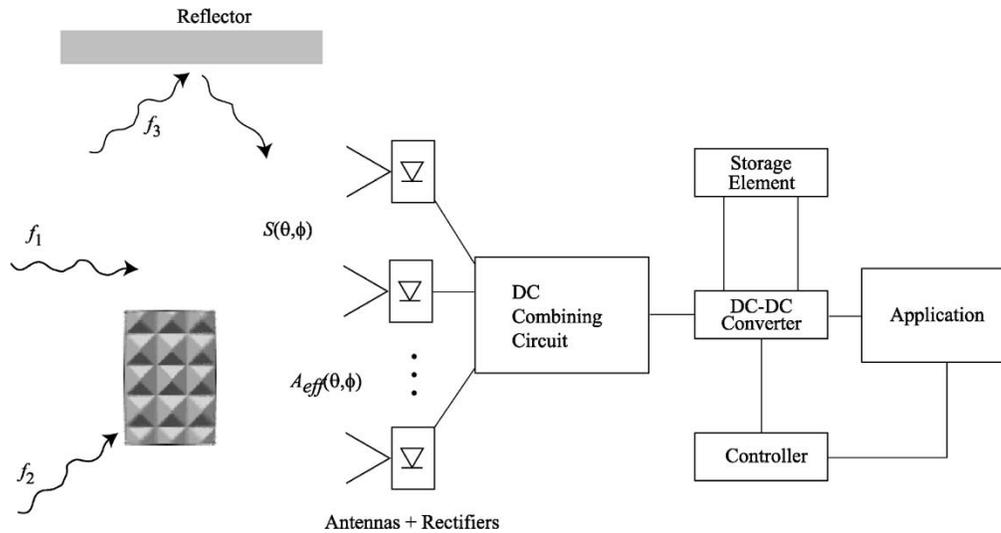

Fig. 2. Block diagram of a rectenna array for ambient energy recycling. Waves of different frequencies and power levels propagate through a complex environment before they are received by a dual-polarized array of antennas. Each element in the array is integrated with a rectifying device. The resulting dc outputs are combined and fed to energy management electronics.

density. A_{eff} is the angle-, frequency-, and polarization-dependent effective area of the antenna. The dc power at a single frequency f_i is given by

$$P_{\text{dc}}(f_i) = P_{\text{RF}}(t, f_i)\eta[P_{\text{RF}}(t, f_i), \rho] \qquad (3)$$

where ρ represents the diode mismatch to the antenna. Due to the nonlinearity of the diode, the mismatch is dependent on power as well as frequency.

The issues related to low-power arbitrarily polarized reception, rectification, and power management are addressed in this paper as follows.

- Section II discusses rectification of low-power microwave signals. Nonlinear simulations of the rectifying device are confirmed with source–pull measurements over a broad frequency range and broad range of input powers. The result is a range of RF impedances presented to the diode for optimal rectification efficiency.
- Section III discusses the design of an antenna integrated with a rectifier. Electromagnetic field simulations are coupled to nonlinear circuit simulations to ensure optimal broad-band match between the antenna and rectifier.

Based on a known range of input power levels, a rectifier diode is chosen from several candidates. Measurements on single rectenna elements are compared to analysis results.
- Section IV describes the design and characterization of a 64-element dual-circular-polarized rectenna array. The frequency response, receive radiation patterns, dc power rectification efficiency, and radiated harmonics are measured. Finally, given the statistical nature of incident RF radiation, the dc rectified power was measured over 10 000 trials with varying frequency and power.
- Section V presents a discussion on storage and management of the extracted dc power with two example applications.

II. MICROWAVE RECTIFICATION AND THE RECTENNA

At low RF frequencies (kilohertz to low megahertz), both p-n diodes and transistors are used as rectifiers. At microwaves (1 GHz and higher), Schottky diodes (GaAs or Si) with shorter transit times are required. In the present case, we have chosen

silicon based on availability, low cost, and simulated performance. Similar to low-frequency, high-power applications, the diode is driven as a half-wave rectifier with an efficiency limited to

$$\eta_{\max} = \frac{1}{1 + \dfrac{V_D}{2V_{\text{out}}}} \tag{4}$$

where V_{out} is the output dc voltage and V_D is the drop across the conducting diode. In this study, it is more appropriate to measure the efficiency defined by (1) which includes the loss due to reflected power.

For low-power applications, as is the case for collected ambient energy, there is generally not enough power to drive the diode in a high-efficiency mode. The diode is not externally biased in this application, so it is important to use a diode with a low turn-on voltage. Furthermore, rectification over multiple octaves requires a different approach from standard matching techniques. In a rectenna application, the antenna itself can be used as the matching mechanism instead of using a transmission-line matching circuit as in [5]–[11]. The antenna design is therefore heavily dependent on the diode characteristics. The following section presents various techniques for analyzing diode operation at microwave frequencies. The results are then used to design the antenna and integrated rectenna for relevant ambient power levels.

A. Analysis and Design Method

A useful time-domain analysis has been applied by McSpadden *et al.* in a number of papers dealing with single-frequency rectennas at microwave frequencies up to the Ka-band [5]. The method uses current–voltage properties of the diode as a basis for predicting rectified power levels and conversion efficiencies. The method has proven to be a successful predictor of conversion efficiencies over a broad range of incident power levels and load impedances. In general, this approach has been used for well-matched diodes integrated with antennas and filters for narrow-band applications.

Several properties of the diode at microwave frequencies require a more comprehensive frequency-domain approach.

1) The nonlinear capacitance of the diode needs to be taken into account past a few gigahertz for most devices.
2) Reflected harmonic energy from the input or output side of the diode can alter the voltage across the diode.
3) The diode begins to bias itself as it produces more dc current, thus moving the dc operating point of the *I–V* curve in a nonlinear fashion.

Certain qualities of microwave rectification can be visualized best in the time domain, i.e., monitoring the complex waveform across the diode. In the frequency domain, the harmonic balance (HB) method of analysis presents a comprehensive treatment of the multispectral problem. Though less helpful diagnostically and heavily dependent on the accuracy of the nonlinear model of the diode, HB provides a tool for addressing all previously mentioned aspects of microwave rectification. The method in-
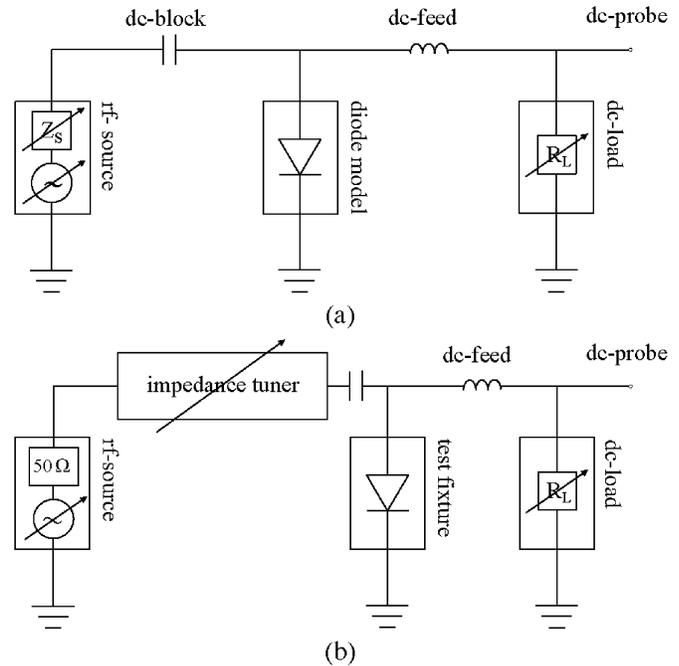

Fig. 3. (a) Circuit diagram of the HB simulation. (b) Diagram of the equivalent source–pull measurement setup.

trinsically takes into account the dc component and a specified number of harmonics, while allowing the ability to specify the source impedance and harmonic terminations.

B. Diode Source–Pull

A source–pull of the diode is a sweep of RF input source impedance values over a given area of the Smith chart. Fig. 3(a) shows the HB simulation approach using Agilent ADS, as well as the measurement approach using impedance tuners. In both simulation and measurements, for a variety of input powers, the resulting dc voltage is quantified for each source impedance and plotted on the Smith chart in Fig. 4. The region of optimal source impedance is later used for optimizing the antenna design so that the antenna presents the proper equivalent source impedance to the diode. In the simulation, an assumption must be made for the impedance seen by the reflected harmonics, and in the presented case this impedance was set to the impedance of a broad-band self-complementary antenna of 189 Ω.

Fig. 4 demonstrates the range of optimal source impedances across the 1–16-GHz range and from -30- to $+10$-dBm input power. The magnitude of the optimal source impedance becomes smaller with increasing incident power. The same occurs as the dc load approaches the optimal value, however, the effect is not as dramatic. More significantly, the optimal source impedance moves counterclockwise along a constant admittance circle with increasing frequency due to the junction capacitance.

The Smith chart plot of Fig. 5 shows a comparison between a simulated source–pull using HB and measurements using a source–pull/load–pull measurement system. A Focus 9-GHz coaxial tuner was used in the measurement setup as described in Fig. 3(b).
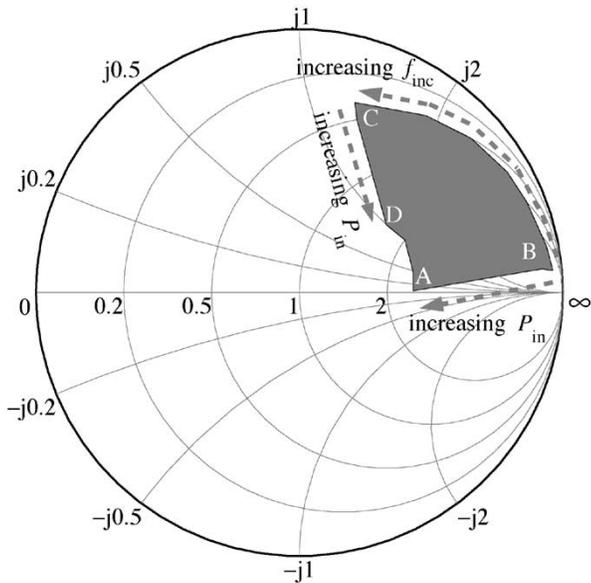
Fig. 4. Simulated range of optimal source impedances for the SMS7630 Schottky diode as the incident wave frequency ($1 \text{ GHz} < f_{\text{inc}} < 16 \text{ GHz}$) and input power ($-30 \text{ dBm} < P_{\text{in}} < +10 \text{ dBm}$) are varied (Smith chart normalized to 50 Ω). Within the shaded area, region A corresponds to high input power and low frequency, B to low power and low frequency, C to low power and high frequency, and D to high power and high frequency.

III. BROAD-BAND RECTENNA DESIGN

Given the good agreement between simulation and experiment, HB was used to evaluate several diodes. The rectification performance is seen to depend most significantly on saturation current, junction capacitance, built-in potential, and series resistance. Fig. 6 shows, qualitatively, regions of high-efficiency performance for three different Schottky diodes obtained by HB simulations. Based on these results, the Alpha Industries SMS7630-079 zero-bias device was selected.

A. Integrated Rectenna Analysis

In most rectenna designs, a narrow-band antenna is used to feed a transmission line followed by space-consuming, traditional matching and filtering sections. In contrast, in the study presented here, the diode is integrated directly into the antenna. Consequently, the antenna is called upon to provide both matching and filtering of the output signal, reducing the required area and increasing the bandwidth. The antenna is included in the HB simulation as the internal impedance of the power source used to drive the circuit. This Thévenin equivalent model allows use of measured or simulated antenna S-parameters in the rectenna simulation [see Fig. 3(a)].

B. Spiral Antenna

As seen in the previous section, the major problem in broad-band rectenna design lies in the nature of the antenna and diode frequency-dependent impedances. For maximal power transfer, the antenna impedance would match the optimal diode impedance for all frequencies. Our approach is to present a
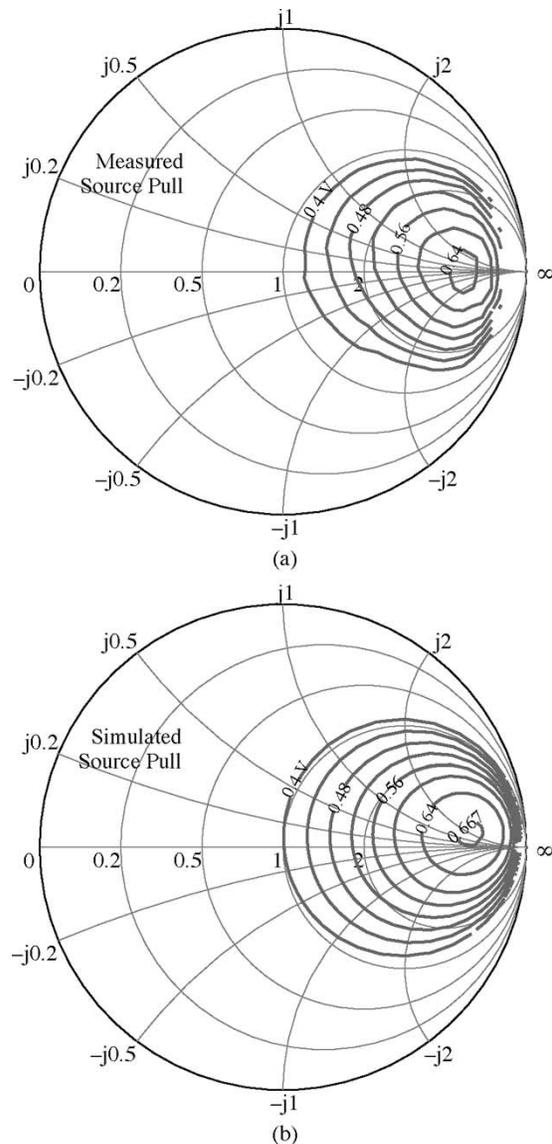

(a)

(b)

Fig. 5. (a) Measured and (b) simulated source–pull of the MA4E2054 diode at 1 GHz. The contours show constant levels of dc voltage over source impedance with constant RF input power (Smith charts normalized to 50 Ω).
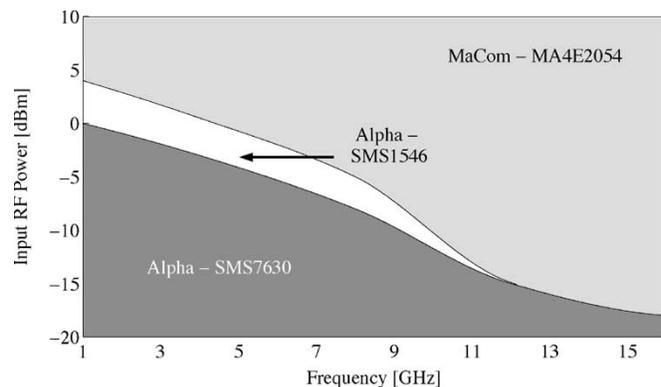

Fig. 6. Simulated qualitative comparison of three commercially available diodes. The different regions in this plot show which diode will have optimal efficiency for a given power and frequency. For the low-power region, the Alpha SMS7630 performs best over the frequency range.

Alpha
SMS7630-079

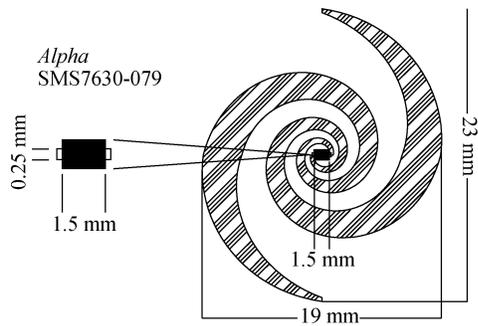0.25 mm
1.5 mm
1.5 mm
19 mm
23 mm

Fig. 7. Layout of the spiral antenna element with a packaged Schottky diode connected directly at the feed. The size of the diode package limits the upper frequency for this broad-band antenna, while the overall antenna size imposes the low-frequency limit.

constant impedance to the diode by using a frequency-independent antenna element.

An equiangular spiral with dimensions shown in Fig. 7 was chosen as the array element for the following reasons:

1) uniplanar with convenient feed point for diode connection;
2) possible dual polarization;
3) convenient connection of dc lines at the tips of the spiral arms.

The spiral element was simulated with full-wave CAD tools (Ansoft's *Ensemble* and Zeland's *IE3D*), resulting in a one-port frequency-dependent impedance that becomes the diode load in the rectenna. The measured impedance of a passive spiral with a coaxial feed-line positioned at the center of the spiral is shown in Fig. 8(a). A diode is then connected at the antenna feed, and the resulting rectenna element performance is shown in Fig. 8(b). The disagreement around 4 GHz is believed to be caused by the 1-cm-long unbalanced coax feed. As a comparison, a second antenna with a balanced feed was characterized and its performance is shown in Fig. 9, indicating broad-band agreement between analysis and measurements. The antenna in this case is a tapered Vivaldi slot with a balanced microstrip feed, and the diode is connected at the feed-point. The simulations are performed with HB and the measured antenna impedance and received power is used in the simulations.

IV. PERFORMANCE OF A BROAD-BAND RECTENNA ARRAY

A 64-element array of left- and right-handed circularly polarized spiral elements is designed, so that each spiral element is directly connected to a rectifier diode. Therefore, the RF powers received independently by each element are summed upon rectification as dc currents and/or voltages. The amount of total rectified power from the array depends on the angle of incidence of the RF plane wave(s). The angle-dependent rectified dc power of a single element can be used to define an *element dc radiation pattern* as follows:

$$G_{dc}(\theta, \phi) = \eta(P_{RF})\frac{4\pi \cdot P_{RF}}{S(\theta, \phi)\lambda^2} = \eta(P_{RF})G(\theta, \phi) \quad (5)$$

where $G(\theta, \phi)$ is the RF radiation pattern. The *dc radiation pattern*, G_{dc}, is different from the RF radiation pattern due to the
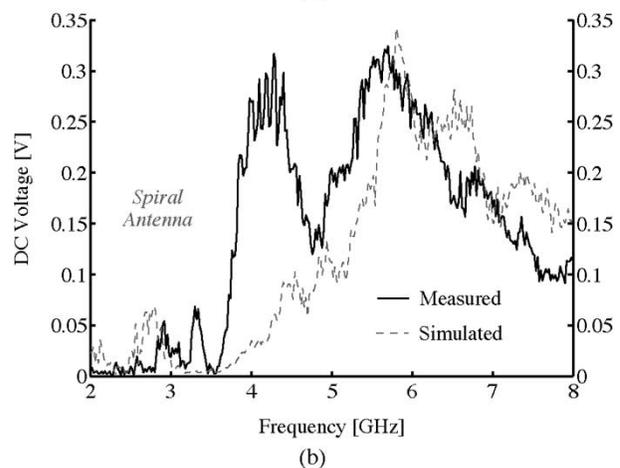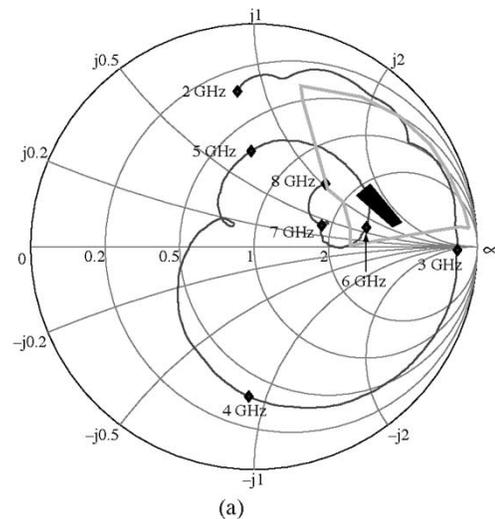

(a)

(b)

Fig. 8. (a) Simulated input impedance of the spiral antenna (normalized to 50 Ω). The optimal region of impedances from Fig. 4 is outlined in gray, and the frequencies and range of input power levels used for this measurement are represented by the black region. (b) Resulting HB simulation and measurements of the dc rectified voltage response across 600 Ω. The incident power on the antenna varies over the frequency range to maintain a constant P_r/G_r ratio as discussed later (cf. Fig. 11).
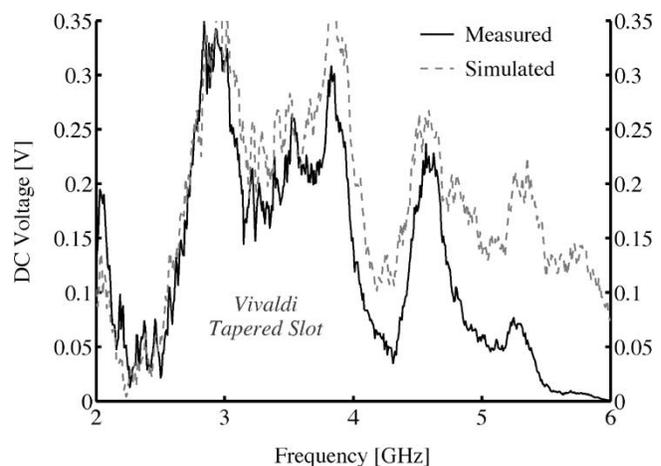

Fig. 9. Simulated and measured rectified voltage across a 600-Ω load as a function of incident RF frequency for a Vivaldi tapered slot with balanced feed.

nonlinear dependence of efficiency on RF power. The resulting pattern obtained by measuring the dc voltage across an optimal
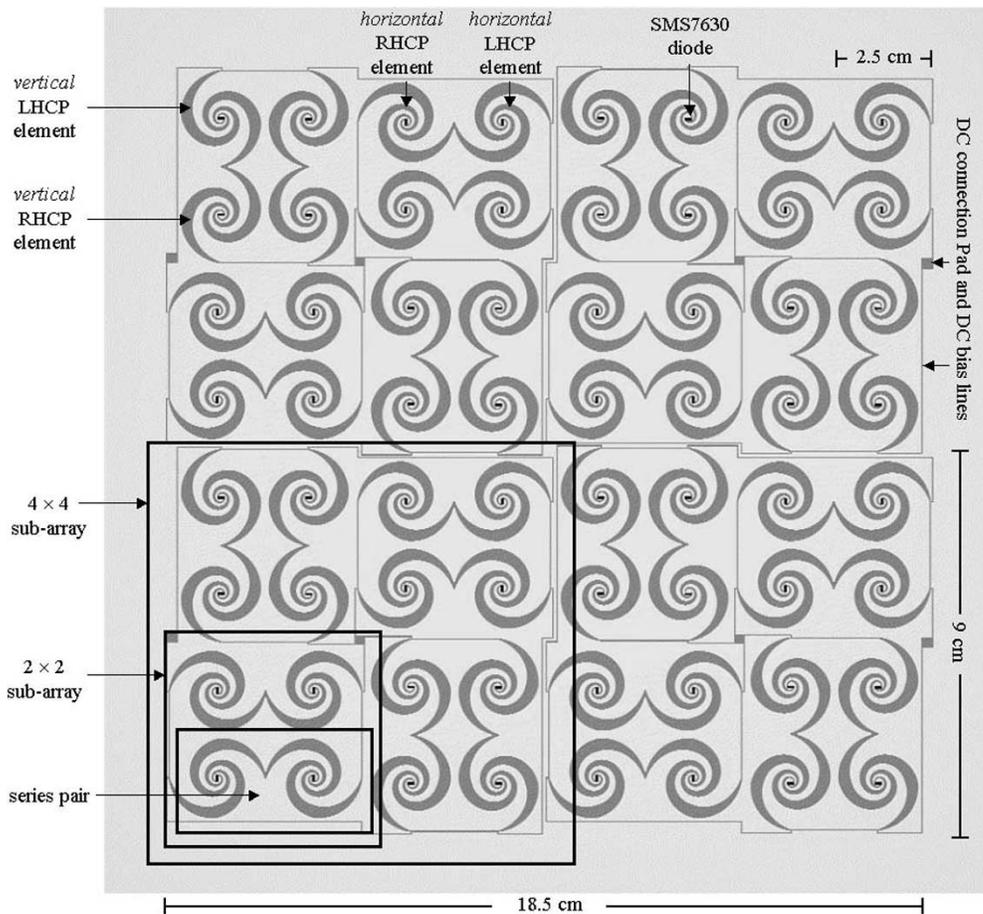
Fig. 10. Layout of the 64-element array. Received RF power is rectified at each spiral locally and the combined dc power for all elements is extracted using two dc collection lines at the edges of the array (not shown). A number of possible dc connections and their effect on efficiency are described in the text.

load exhibits lower gain at larger angles θ and ϕ. The radiation pattern for the n-element array is given by

$$G_{\text{dc}}^m(\theta, \phi) = \kappa(P_{\text{RF}})G_{\text{dc}}(\theta, \phi) \qquad (6)$$

where κ is a function of incident RF power and dc combining circuit. To first order, κ is not a function of incidence angle.

A. Array Design

Fig. 10 shows the array layout. At lower frequencies, the increased mutual coupling between elements and the presence of the dc collection lines increases the power delivered to the diodes by increasing the effective aperture of each element. The problem of polarization performance is addressed by alternating left and right circular polarization between neighboring elements and by an additional rotation of 90° from element to element. This means that the array suffers an average 3-dB input polarization loss for *every* possible polarization of the incident energy. However, this strategy ensures a flat polarization response.

The crucial design step for the array is to achieve optimal dc combining efficiency. Previous work shows that predominantly parallel connections (current-summing) lead to smaller matched loads for the rectenna [19]. For a series-connected array (voltage-summed), the matched load is much higher. This can be seen by reducing the array to a combination of

dc Thévenin sources where the matched load corresponds to the total source resistance. The nonlinear performance of the diodes must again be considered when considering the dc connections. Increased current or voltage in a predominately series or parallel-connected array can lead to over-biasing of the individual diodes such that the rectification process is uniformly degraded over the array. Furthermore, the dc power level is very sensitive to under illumination. For these reasons, the 64-element array is connected using 2×1 parallel pairs connected in series to form a 2×2 subarray: four of these are connected in parallel to create a 4×4 subarray: four more of these are then left as units to comprise the 8×8 array with reconfigurable connectivity.

B. Frequency Response

The frequency dependence is measured in two ways: three-dimensional patterns are integrated from 2 to 8 GHz where sufficient power was available for the measurement. Since the radiation patterns are reasonably smooth, only the broadside frequency response was measured. Higher input powers were used for 2–8 GHz and a low power level was used for the broad range from 2 to 18 GHz. The broadside frequency response was also measured using a uniform incident power density to synthesize constant input power to the diodes. The results for three input power levels are shown in Fig. 11.
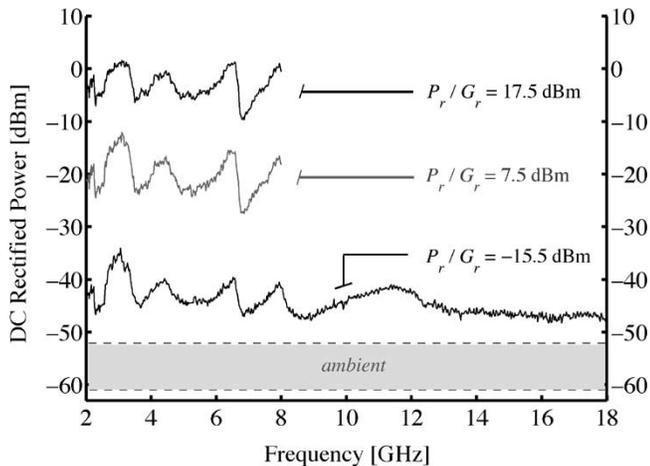
Fig. 11. Measured broad-band frequency response for various incident power levels related to the power density S by $P_r/G_r = S\lambda^2/(4\pi)$. The shaded area represents the range of rectified power levels resulting from an ambient RF background signal present in the building.
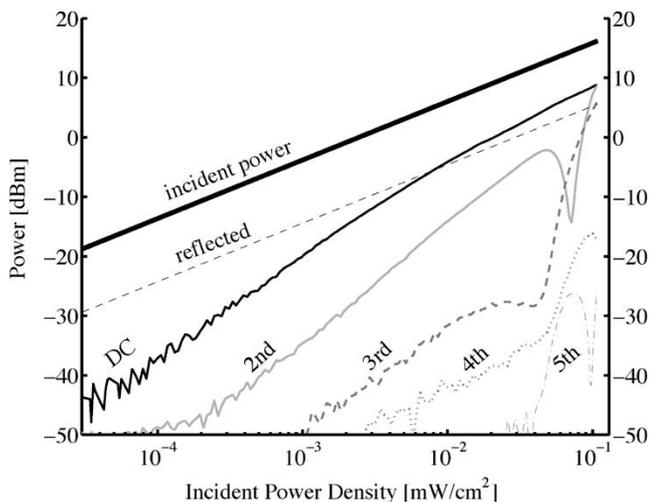

Fig. 12. Measured reflected, rectified, and reradiated harmonic power as a function of incident power density. The conversion efficiency ranges from 0.1% for an incident power density of $5 \cdot 10^{-5}$ mW/cm^2 to 20% for an incident power density of 0.07 mW/cm^2 (also indicated in Fig. 1).

C. DC-Power Response and Radiated Harmonics

To gain a better understanding of the nonlinear power dependence of the rectenna, a sweep of the input power is performed and the resulting dc output and reradiated powers are quantified. The measurement, summarized in Fig. 12, is made with broadside linearly polarized radiation at 3 GHz with incident power densities ranging from tens of nW/cm^2 to 0.1 mW/cm^2. The rectenna array receives radiation from all directions (there is no ground plane), and, in order to measure the reradiated power at the harmonics, the array was placed half way between a transmit and receive test antenna, perpendicular to the line-of-sight axis. The dc voltage is extracted with dc collection lines and measured across a 100-Ω load. The rectification efficiency reaches the 20% range for an incident power density of 0.1 mW/cm^2 and arbitrary polarization.

Also shown in Fig. 12 is the relative amount of reflected power along with the radiated power of the second through fifth harmonics. The reflected power is found from a time-gated S_{11}-measurement using a vector network analyzer. The result, consistent with simulation results, indicates that the reflected power varies linearly with input power up to 0.1 mW/cm^2. Simulations suggest, however, that the reflections begin to drop as higher power levels are applied and a larger fraction of incident power is converted to dc and power at the harmonics.

For different dc connections, the diodes across the array are biased at different quiescent points on the diode $I–V$ curve. Table I shows efficiency measured across a 600-Ω load for a 2×2 subarray and the 8×8 array with three dc-connection schemes for incident power densities at the lower and upper ends of the range indicated in Fig. 1. Quartiles are defined as the 4×4 subarrays. For this array, the parallel configuration of the subarrays gave the highest efficiency over the range of incident power densities.

D. DC Receive Patterns and Polarization

The patterns of the rectenna array are found by measuring the output dc rectified power over a hemisphere sampled at 1012 points (see Figs. 13 and 14). These patterns are a superposition of the response to two orthogonally linearly polarized incident waves. At higher frequencies, the spiral element is predominately circularly polarized. In order to design a broad-band array with as uniform a pattern in space and polarization as possible, right-hand and left-hand circularly polarized spirals are alternated in the layout. The planar layout of the array places certain limits on the polarization and reception at azimuth angles. Figs. 13 and 14 show that the radiation pattern has low directivity and is similar to that of a single element. Note that the size of the array is $1.5\lambda_o^2$ at 2 GHz and $116\lambda_o^2$ at 18 GHz. However, by observing the patterns in Figs. 13 and 14, it is seen that the array receives from all directions over a broad frequency range.

E. Statistical Study of Multitone Performance

As a final test, the array is placed in a controlled, multitone environment. The point of this test is to demonstrate how the dc response improves or degrades when several waves of more than one frequency are incident simultaneously. Two signal sources, separated by 20° in an incidence angle from the rectenna and 45° in polarization, are used to represent multiple inputs with variable frequency and power. In order to ensure uncorrelated input waves, paired frequencies and power levels are generated randomly with a uniform distribution using MATLAB.

The experiment is run by first generating one randomized frequency between 2–8 GHz and one incident power level between approximately 0.1 μW/cm^2 and 0.1 mW/cm^2. Each source is turned on separately to record the independent dc rectified powers. Both sources are then turned on simultaneously and the new rectified power is recorded. This process is repeated for 10 000 randomized input pairs. The sums of the two independent rectified powers for each trial were then sorted by magnitude and compared with the corresponding rectified power from the simultaneous illumination from both sources.

TABLE I
RECTIFICATION EFFICIENCY FOR A 2 × 2 SUBARRAY AND THE 8 × 8 ARRAY WITH THREE DC-CONNECTION SCHEMES FOR INCIDENT POWER
DENSITIES AT THE LOWER AND UPPER ENDS OF THE RANGE INDICATED IN FIG. 1. QUARTILES ARE DEFINED AS THE 4 × 4 SUBARRAYS

power density [mW/cm^2]	2×2 2 elements in series, 2 parallel	8×8 2 quartiles in series, 2 parallel	8×8 quartiles all in parallel	8×8 quartiles all in series
$S = 6.2 \cdot 10^{-2}$	0.4%	16%	20%	13%
$S = 6.2 \cdot 10^{-4}$	0.03%	1.1%	2.3%	0.95%

Fig. 13. Measured dc power as a function of angle of incidence over a hemisphere for two orthogonally linearly polarized input waves at 2 GHz. The pattern is related to an RF radiation pattern through (5) and (6).
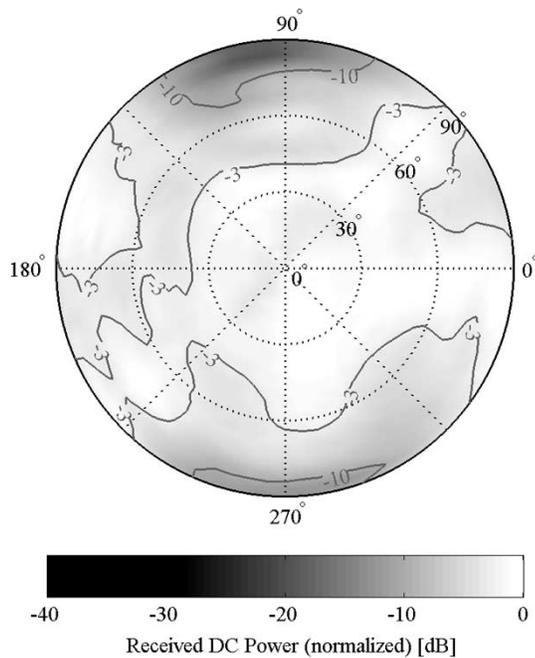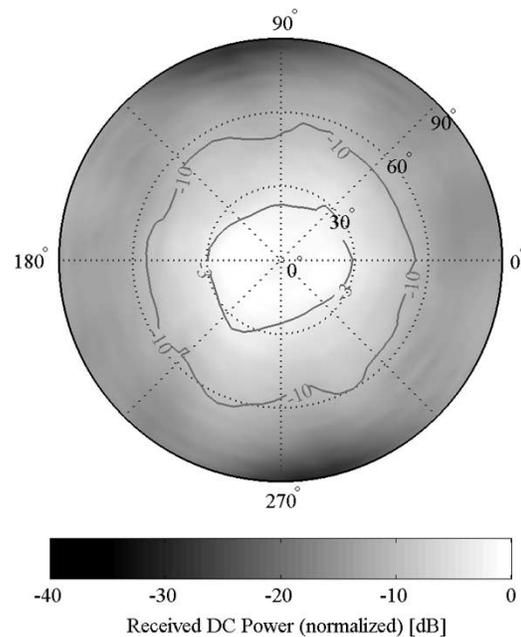

Fig. 14. Measured dc power as a function of angle of incidence over a hemisphere for two orthogonally linearly polarized input waves at 4.6 GHz. The pattern is related to an RF radiation pattern through (5) and (6).

The result, shown in Fig. 15, reveals the phenomenon that the independent sources combine nonlinearly, when simultaneously incident, to produce *more* rectified power in *every* instance. When the total input power is low, the average increase due to simultaneous illumination is higher. The mean increase for three ranges in incident power level is indicated in the figure. This correlation is much stronger than the frequency or incident power correlation. For this reason, Fig. 15 was plotted according to P_{indep}. Also shown is the mean increase in power for three portions of the curve.

It should also be noted that, in general, the power increase diminishes as the two frequencies approach one another. Furthermore, local power-increase minima occur for certain difference frequencies, i.e., $|\Delta f|$. This is thought to be due to a spiral input impedance which efficiently radiates the difference frequency rather than further rectifying the energy.

V. ENERGY STORAGE AND MANAGEMENT FOR LOW-POWER APPLICATIONS

A study of rectification of broad-band statistically varying RF radiation is presented in this paper. The experimental results show that the combined electromagnetic field analysis for the
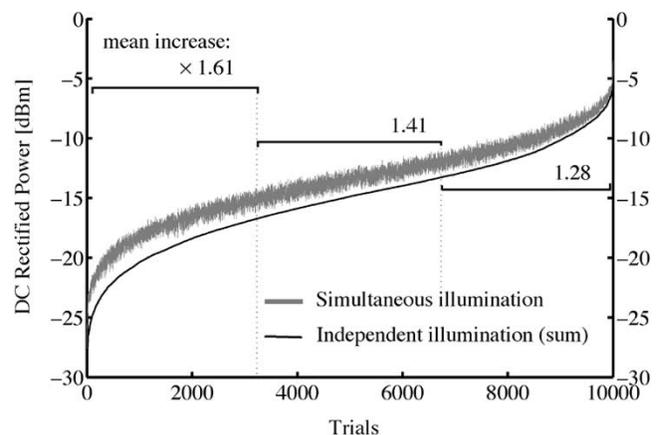

Fig. 15. Comparison of total rectified power for independent and simultaneous dual-frequency illumination as explained in Section IV-E. The results of 10 000 trials are rank ordered by dc power to illustrate the power-dependent increase in rectification efficiency.

radiating element and HB nonlinear circuit simulations result in predictable rectenna performance. The work focuses on arbitrary polarized low incident power density reception and rectification and shows that rectification efficiencies with average 20% over time, frequency, and polarization are achieved.
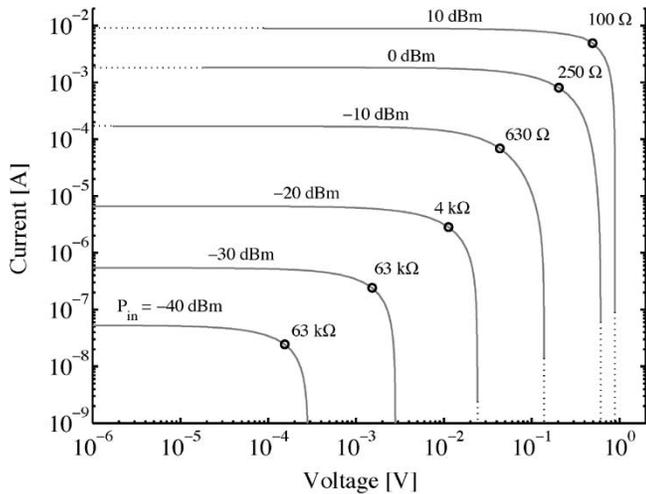
Fig. 16.   Simulated *I–V* curves as a function of load resistance and input RF power to the diode. The peaks in rectified power are indicated by circles with the corresponding optimal load resistance.

If one of these requirements is relaxed, i.e., high-power, narrow-band, linearly polarized, and/or time-constant power is transmitted, higher efficiencies up to 60% at the X-band [5] can be expected. The motivation for considering the low-power random case are applications in ambient energy recycling and low-power batteryless sensors.

The first type of application addresses using otherwise wasted power, which in some cases can also help reduce health hazards. For example, the rooftops of buildings in city centers are often leased to a number of wireless providers and technical staff has reported health problems when servicing a transmitter in the presence of other operating transmitters [18]. In this environment, a variety of output powers, frequencies, and polarizations are present, and interference between a number of antennas in each other's near fields changes their radiation properties, accounting for more *wasted* power. The results of this paper show that this power can be absorbed (received), rectified, and stored for future use.

Fig. 1 shows the more typical levels of ambient power densities in the microwave frequency range, with power levels that are too low for most continuous electronic functions. However, if this energy is stored over time efficiently, realistic functions can be performed in discrete time intervals. The ambient RF power levels vary by several orders of magnitude, implying a varying dc load as reflected in the *I–V* characteristics of a single rectenna element, shown in Fig. 16. For maximum dc power generation, it is necessary to either match the output characteristics of the source with the load or to insert an intermediate dc–dc converter with peak power tracking. Many techniques for low-power dc–dc conversion are described in [20], with an emphasis on pulsewidth modulated (PWM) converters. Traditional PWM converters are likely to consume far too much power in the control and gate drive circuitry and/or require large off-chip inductor(s) for low-frequency operation. As an alternative, switched-capacitor (SC) converters can provide high efficiency conversion at low power levels over a discrete range of conversion ratios determined by the circuit size and complexity

[21]. Although parasitics in silicon processing have limited efficiency of SC converters, recent advances in technologies such as fully depleted silicon-on-insulator have enabled fully integrated efficiencies of greater than 90% [22].

Referring to the block diagram in Fig. 2, two options for energy storage include capacitors and micro-batteries [23]. Capacitive energy storage is appropriate for applications where repeated functions of storing and utilizing small energy packets is performed, using on-chip (up to tens of picojoules of off-chip, up to tens of microjoules) capacitors. For prolonged operation or larger energy packets, energy densities up to four orders of magnitude higher can be achieved using micro-batteries [24].

To illustrate the application of the rectenna energy source, we consider the ability to generate 10-μJ energy packets, which is sufficient for a 1-mW 10-μs load operation. The energy packet size was selected arbitrarily but could be used, for example, for RF transmission of up to 10-kb data packets or simple sensory and signal processing functions. Over the range of incident power densities under consideration (see Fig. 1) and assuming an array of

$$A = A_{\mathrm{eff}} = 25 \ \mathrm{cm}^2 \tag{7}$$

we estimate incident power levels of

$$P_{\mathrm{RFmin}} = 250 \ \mathrm{nW} \quad P_{\mathrm{RF\,max}} = 2.5 \ \mathrm{mW}. \tag{8}$$

Assuming a dc–dc conversion efficiency of 90% and rectification efficiencies of

$$\eta(P_{\mathrm{RFmin}}) = 1\% \quad \eta(P_{\mathrm{RFmax}}) = 20\% \tag{9}$$

an average dc power output is obtained as

$$P_{\mathrm{dcmin}} = 2 \ \mathrm{nW} \quad P_{\mathrm{dc\,max}} = 450 \ \mu\mathrm{W}. \tag{10}$$

The above estimated power levels can be recycled using this kind of a device. In another important application, batteryless sensors, this power is used to transmit power from this sensor. There are two possible scenarios, which are: 1) vary integration time to achieve fixed energy level and 2) fix integration time and vary energy packet level. Following approach 1), the system would be capable of fixed 10-μJ operation at discrete intervals varying from 1.4 h in the worst case to 20 ms in the best case. Thus, if a simple sensor required one energy packet to perform the sensory function and one packet to transmit data, it would be able to transmit new data around 20 times per second in the best case.

An example of the latter application is a manufacturing environment, where a large number of sensors occasionally transmit data such as stress, temperature, pressure, and light level. A large number of such sensors with no batteries that need replacing (or recycling) can be charged with a low-power transmitter overnight. In such an indoor multipath propagation environment, the spatial distribution of polarization and power varies statistically. The results of this paper show that it is possible to efficiently collect such energy by receiving and rectifying two orthogonal polarizations independently and adding the power upon rectification.

REFERENCES

[1] W. C. Brown, "The history of power transmission by radio waves," *IEEE Trans. Microwave Theory Tech.*, vol. MTT-32, pp. 1230–1242, Sept. 1984.

[2] N. Shinohara and H. Matsumoto, "Experimental study of large rectenna array for microwave energy transmission," *IEEE Trans. Microwave Theory Tech.*, vol. 46, pp. 261–267, Mar. 1998.

[3] J. O. McSpadden, F. E. Little, M. B. Duke, and A. Ignatiev, "An in-space wireless energy transmission experiment," in *Proc. IECEC Energy Conversion Engineering Conf.*, vol. 1, Aug. 1996, pp. 468–473.

[4] K.Kai Chang, *Microwave Ring Circuits and Antennas*. New York: Wiley, 1996.

[5] T. Yoo and K. Chang, "Theoretical and experimental development of 10 and 35 GHz rectennas," *IEEE Trans. Microwave Theory Tech.*, vol. 40, pp. 1259–1266, June 1992.

[6] L. W. Epp, A. R. Khan, H. K. Smith, and R. P. Smith, "A compact dual-polarized 8.51-GHz rectenna for high-voltage (50 V) Actuator applications," *IEEE Trans. Microwave Theory Tech.*, vol. 48, pp. 111–120, Jan. 2000.

[7] Y. Fujino, T. Ito, M. Fujita, N. Kaya, H. Matsumoto, K. Kawabata, H. Sawada, and T. Onodera, "A driving test of a small DC motor with a rectenna array," *IEICE Trans. Commun.*, vol. E77-B, no. 4, pp. 526–528, Apr 1994.

[8] W. C. Brown, "An experimental low power density rectenna," in *IEEE MTT-S Int. Microwave Symp. Dig.*, 1991, pp. 197–200.

[9] J. O. McSpadden, I. Fan, and K. Chang, "A high conversion efficiency 5.8-GHz rectenna," *IEEE Trans. Microwave Theory Tech.*, vol. 46, pp. 2053–2060, Dec. 1998.

[10] J. O. McSpadden and K. Chang, "A dual polarized circular patch rectifying antenna at 2.45 GHz for microwave power conversion and detection," in *IEEE MTT-S Int. Microwave Symp. Dig.*, 1994, pp. 1749–1752.

[11] B. Strassner and K. Chang, "A circularly polarized rectifying antenna array for wireless microwave power transmission with over 78% efficiency," in *IEEE MTT-S Int. Microwave Symp. Dig.*, 2002, pp. 1535–1538.

[12] P. Foster and R. Burberry, "Antenna problems in RFID systems," in *Proc. IEE Colloq. RFID Technology*, vol. 3, Oct. 1999, pp. 1–5.

[13] S. Wu, J. Yang, and T. Liu, "A transponder IC for wireless identification systems," in *Proc. 7th IEEE Int. Personal, Indoor, and Mobile Radio Communications Symp.*, vol. 1, Oct. 1996, pp. 238–241.

[14] H. Matsuki, Y. Yamakata, and N. Chubachi, "Transcutaneous DC–DC converter for totally implantable artificial heart using synchronous rectifier," *IEEE Trans. Magn.*, vol. 32, pp. 5118–5120, Sept. 1996.

[15] J. Parramon, P. Doguet, D. Marin, M. Verleyssen, R. Munoz, and L. Leija, "ASIC-based batteryless implantable telemetry microsystem for recording purposes," in *Proc. IEEE/EMBS Int. Conf.*, 1997, pp. 2225–2228.

[16] J. C. Lin, "Radio frequency exposure and safety associated with base stations used for personal wireless communication," *IEEE Antennas Propagat. Mag.*, vol. 44, no. 1, pp. 180–183, Feb. 2002.

[17] ——, "Space solar-power stations, wireless power transmissions, and biological implications," *IEEE Microwave Mag.*, pp. 36–42, Mar. 2002.

[18] J. A. Hagerty and Z. Popović, "An experimental and theoretical characterization of a broadband arbitrarily-polarized rectenna array," in *IEEE MTT-S Int. Microwave Symp. Dig.*, vol. 3, 2001, pp. 1855–1858.

[19] N. Shinohara and H. Matsumoto, "Dependence of dc output of a rectenna array on the method of interconnection of its array elements," *Elect. Eng. Japn.*, vol. 125, no. 1, pp. 9–17, 1998.

[20] A. Stratakos, R. Sullivan, S. Sanders, and R. Broderson, "High-efficiency low-voltage dc–dc conversion for portable applications," in *Low-Voltage/Low-Power Integrated Circuits and Systems*. Piscataway, NJ: IEEE Press, 1999, ch. 12.

[21] M. Makowski and D. Maksimović, "Performance limits of switched-capacitor dc–dc converters," in *Proc. IEEE Power Electronics Specialists Conf.*, 1995, pp. 1215–1221.

[22] J. Kajiwara, M. Kinoshita, S. Sakiyama, and A. Matsuzawa, "High efficiency and latch-up free switched capacitor up converter on FD-SOI technology," in *Proc. IEEE Symp. VLSI Circuits*, 2002, pp. 288–291.

[23] P. Koeneman, I. Busch-Vishniac, and K. Wood, "Feasibility of micro power supplies for MEMS," *J. Microelectromech. Syst.*, vol. 5, pp. 355–362, Dec. 1997.

[24] R. LaFollette, J. Harb, and P. Humble, "Microfabricated secondary batteries for remote, autonomous, electronic devices," in *Proc. IEEE 16th Annu. Batter Applications and Advances Conf.*, 2001, pp. 349–354.

Joseph A. Hagerty (S'96) was born in Houston, TX, in 1973. He received the B.S. degree in electrical engineering from the University of Houston, Houston, TX, in 1998, and the M.S. and Ph.D. degrees in electrical engineering from the University of Colorado at Boulder, in 2001 and 2003, respectively.

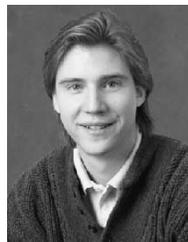He is currently with dBm Engineering, Boulder, CO.

Florian B. Helmbrecht (S'02) received the Dipl.-Ing. degree from the Technical University of Munich, Munich, Germany in 2002, and is currently working toward the Dr.-Ing. degree at the Technical University of Munich.

In 2002, he was with the University of Colorado at Boulder, where he performed research. His current research activities include three-dimensional radar imaging.

William H. McCalpin (S'01) received the B.S.E.E. degree from the University of California at Santa Barbara, in 1987, and the M.S.E.E. degree in semiconductor devices and microwave circuits from Santa Clara University, Santa Clara, CA, in 1994.

In 2000, he founded dBm Engineering Inc., Boulder, CO. He has been extensively involved with high-power RF amplifiers and discrete power devices. He holds five patents related in these areas.

Regan Zane (M'99) received the B.S., M.S., and Ph.D. degrees in electrical engineering from the University of Colorado at Boulder, in 1996, 1998, and 1999, respectively.

He is currently an Assistant Professor of electrical engineering with the University of Colorado at Boulder. From 1999 to 2001, he was a Research Engineer with the Global Research Center, General Electric, where he developed mixed-signal integrated-circuit (IC) controllers for electronic ballasts. In 2001, he joined the faculty of the University of Colorado at Boulder and became a Research Advisor with the Colorado Power Electronics Center. His research interests include mixed-signal IC design for-power converters, modeling and analysis of switching converters, and power generation and management in low-power wireless systems.

Dr. Zane was the recipient of a 2004 National Science Foundation (NSF) CAREER Award.

Zoya B. Popović (S'86–M'90–SM'99–F'02) received the Dipl. Ing. degree from the University of Belgrade, Serbia, Yugoslavia, in 1985, and the Ph.D. degree from the California Institute of Technology, Pasadena, in 1990.

Since 1990, she has been with the University of Colorado at Boulder, where she is currently a Full Professor. She has developed five undergraduate and graduate electromagnetics and microwave laboratory courses and coauthored (with her father) the textbook *Introductory Electromagnetics* (Upper Saddle River, NJ: Prentice-Hall, 2000) for a junior-level core course for electrical and computer engineering students. Her research interests include microwave and millimeter-wave quasi-optical techniques, high-efficiency microwave circuits, smart and multibeam antenna arrays, intelligent RF front ends, RF optical techniques, batteryless sensors, and broad-band antenna arrays for radio astronomy.

Dr. Popović was the recipient of the 1993 Microwave Prize presented by the IEEE Microwave Theory and Techniques Society (IEEE MTT-S) for the best journal paper. She was the recipient of the 1993 National Science Foundation (NSF) Presidential Faculty Fellow Award. She was the recipient of the 1996 URSI Isaac Koga Gold Medal. In 1997, Eta Kappa Nu students chose her as a Professor of the Year. She was the recipient of a 2000 Humboldt Research Award for Senior U.S. Scientists from the German Alexander von Humboldt Stiftung. She was also the recipient of the 2001 Hewlett-Packard (HP)/American Society for Engineering Education (ASEE) Terman Award for combined teaching and research excellence.